CDRI ◇

UNDP

Global Infrastructure Resilience
Capturing the Resilience Dividend

Supplement material to the GIRI global flood hazard model

CIMA Foundation, Italy

Position Paper | 2023

cima
RESEARCH
FOUNDATION

Supplement of

The GIRI global flood hazard model

Lorenzo Alfieri, Lorenzo Campo, Simone Gabellani, Tatiana Ghizzoni, Christian Herold, Andrea Libertino, Eva Trasforini, and Roberto Rudari

[1]CIMA Research Foundation, Savona, Italy
[2]UNEP/GRID, Geneva, Switzerland

Correspondence to: Lorenzo Alfieri (lorenzo.alfieri@cimafoundation.org)

Model selection for future climate projections

The variability of the temperature change among the different models/scenarios is very large, thus, in order to reach a compromise between a proper representation of this variability and the available computational resources, a selection was made.

Figure S1: Schematics for the climatic model bounds selection.

Table S1: CMIP6 climate models included in ISIMIP3b.

Model	Group	Resolution	Member	piControl	ps	sfcWind
GFDL-ESM4	primary	1.0°	r1i1p1f1	0001–0500	available	available
IPSL-CM6A-LR	primary	2.0°	r1i1p1f1	1870–2369	available	available
MPI-ESM1-2-HR	primary	1.0°	r1i1p1f1	1850–2349	available	available
MRI-ESM2-0	primary	1.0°	r1i1p1f1	1850–2349	proxy	available
UKESM1-0-LL	primary	2.0°	r1i1p1f2	1960–2459	available	available
CanESM5	secondary	2.0°	r1i1p1f1	5201–5700	proxy	available
CNRM-CM6-1	secondary	1.0°	r1i1p1f2	1850–2349	proxy	proxy
CNRM-ESM2-1	secondary	1.0°	r1i1p1f2	1850–2140	proxy	proxy
EC-Earth3	secondary	0.5°	r1i1p1f1	2259–2758	proxy	available
MIROC6	secondary	1.0°	r1i1p1f1	3200–3699	proxy	proxy

When future climate is considered, different General Circulation Models (GCM) are available for different SSP scenarios. In the case of the ISIMIP3b dataset, 15 different combinations are available, based on 3 SSP/RCP and 5 climate models.

Given the limited resources available for the study it was not possible to run the global risk computations for every hazard, every exposure element for all the members of the climate ensemble, even if that would have been the optimal choice in case of sufficient resources. To reduce the computational load, a subset of the available runs must be selected according to meaningful criteria. In this case the intent of the global probabilistic risk model is to provide sensible bounds to the risk figures in the different areas of the world. The uncertainty in future climate projection is different in nature and can be reconducted on one side to the uncertainties that are brought by the specific numerical model used for the prediction, and on the other side to our inability in guessing what scenario of greenhouse gas emissions connected to a specific socio-economic development pathway will materialize in future. From the risk assessment perspective both sources of uncertainty should be considered explicitly, therefore the selection of the bounding climate scenarios should be independent from the modeling suite and SSP considered. Therefore, all possible combination should be analyzed and the most impactful and the less impactful selected, irrespective of the specific model or SSP considered. To preselect the runs used in the risk computations, a combined analysis at global scale of the temperature and the precipitation trends has been performed to identify the runs able to produce the maximum variation of the risk figures for the different hazards. It is expected that hazard like Floods, Cyclones and rainfall-induced landslides would be highly correlated with strong increase in precipitation, while hazards like droughts will be strongly correlated with the increase in temperature. The correlation among temperature and precipitation trends enabled us to use 2 reference runs consistent throughout the different hazards (Figure 24).

Two scenarios were chosen, adopting as criterion a statistical selection based on the percentiles of the ensemble of temperature trajectories (precipitation trends are perfectly correlated with the trends in temperature for all the different models and SSPs). For each year of the future projection period (2017-2100), the 20-percentile and 80-percentile of the ensemble of average world temperature on land were computed, yielding two additional temperature trajectories produced as the 20-percentile and 80-percentile ensemble mean. Then, the most similar simulation, among the model runs available, was selected for each of the two percentiles. These two combinations of GCM/SSP were used to characterize the climate change variability without having to deal with the whole ensemble. This exercise was repeated for each single continent in order to reveal possible inconsistencies or specific behaviors

of model runs in the different areas of the world. The run selection showed to be consistent throughout the continents therefore 2 reference simulations for the future climate were selected.
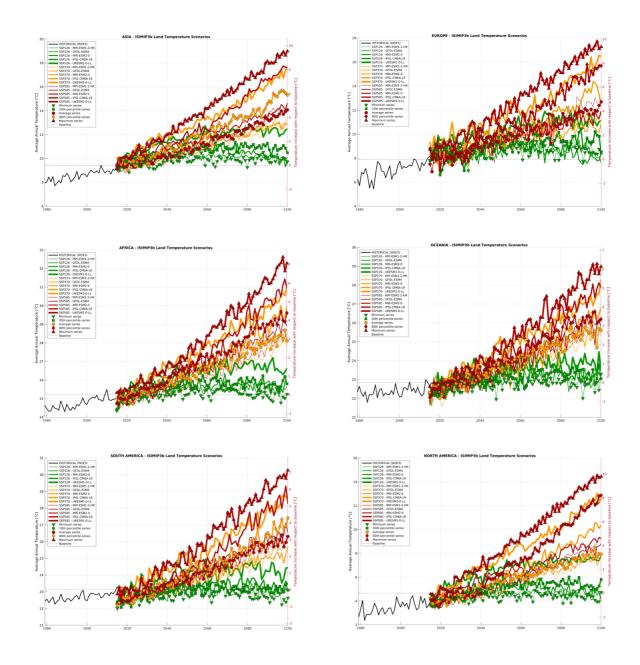
Figure S2: Statistical analysis of the continental temperature trends.

The selected simulations were SSP126/IPSL-CM6A-LR for 20-percentile (low scenario) and SSP585/IPSL-CM6A-LR for 80-percentile (high scenario) (see Figure 26 for a complete view of the model selection).

	Africa	Asia	Europe	North America	South America	Oceania	Land	World
Minimum series	SSP126-MPI-ESM1-2-HR	SSP126-MPI-ESM1-2-HR	SSP126-MPI-ESM1-2-HR	SSP126-MPI-ESM1-2-HR	SSP126-MPI-ESM1-2-HR	SSP126-MPI-ESM1-2-HR	SSP126-MPI-ESM1-2-HR	SSP126-MPI-ESM1-2-HR
20th percentile	SSP126-IPSL-CM6A-LR	SSP126-IPSL-CM6A-LR	SSP126-IPSL-CM6A-LR	SSP126-IPSL-CM6A-LR	SSP126-MRI-ESM2-0	SSP126-MRI-ESM2-0	SSP126-IPSL-CM6A-LR	SSP126-IPSL-CM6A-LR
Average series	SSP370-GFDL-ESM4	SSP585-GFDL-ESM4	SSP585-GFDL-ESM4	SSP370-MRI-ESM2-0	SSP585-MRI-ESM2-0	SSP370-MRI-ESM2-0	SSP370-MRI-ESM2-0	SSP370-MRI-ESM2-0
80th percentile	SSP585-MRI-ESM2-0	SSP370-IPSL-CM6A-LR	SSP585-IPSL-CM6A-LR	SSP585-IPSL-CM6A-LR	SSP370-IPSL-CM6A-LR	SSP585-MRI-ESM2-0	SSP370-IPSL-CM6A-LR	SSP585-IPSL-CM6A-LR
Maximum series	SSP585-UKESM1-0-LL	SSP585-UKESM1-0-LL	SSP585-UKESM1-0-LL	SSP585-UKESM1-0-LL	SSP585-UKESM1-0-LL	SSP585-UKESM1-0-LL	SSP585-UKESM1-0-LL	SSP585-UKESM1-0-LL

Figure S3: Climate model selection analysis for the different domains considered.

The meteorological datasets used for hydrological simulations are listed in Table S2.

Table S2. Meteorological datasets used as input of the Continuum hydrological model.

Dataset	Use	Characteristics
W5E5	Meteo input for historical period	Global meteorological dataset, variables used: precipitation, near surface air temperature, near surface air humidity, near surface wind velocity, surface solar radiation (Time resolution: daily, Time period availability: 1979-2016, Spatial resolution: 0.5°)
ISIMIP3b	Meteo input for future period (SSP scenarios)	Global scale climate projection dataset, available for historic runs and future SSP scenarios. Bias-corrected using ISIMIP3BASD v2.5. Variables used: precipitation, near surface air temperature, near surface air humidity, near surface wind velocity, surface solar radiation (Time resolution: daily, Time period availability: 2017-2100, Spatial resolution: 0.5°)

Static data

Static data used in the global implementation of the Continuum model are reported in Table S3.

Table S3. Continuum static data and sources

Data	Source	Reference
DEM	MERIT-Hydro database	(Yamazaki et al., 2019)
Soil texture map	SoilGrids Sand Content - SoilGrids Clay Content	(Hengl et al., 2017)
Lakes characteristics	HydroLAKES v1.0 database	(Messager et al., 2016)
Dams characteristics	Global Reservoir and Dam Database (GRanD v1.3)	(Lehner et al., 2011)
Land use and vegetation coverage	ESA-CCI C3S Global Land Cover	(ESA, 2017)
River width and depth	Global database by Andreadis et al. (2016)	(Andreadis et al., 2013)

Table S4. Continuum static data maps

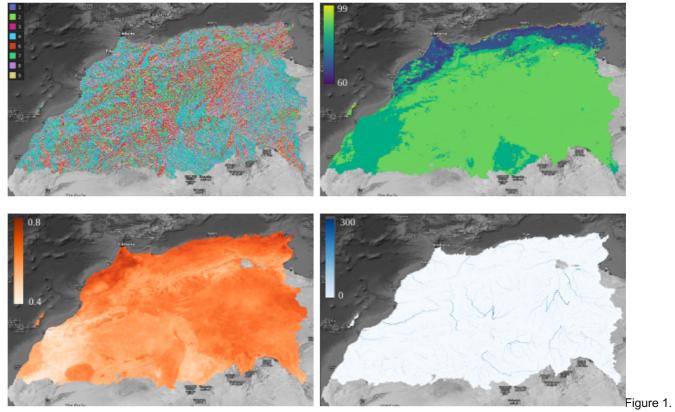| Name	Description	Type
{domain}.dem	Digital Elevation Model	Grid
{domain}.pnt	Drainage direction	Grid
{domain}.choice	Channel network	Grid
{domain}.area	Upstream area	Grid
{domain}.areacell	Area of grid cell	Grid
{domain}.lat	Latitude of grid cell	Grid
{domain}.lon	Longitude of grid cell	Grid
{domain}.alpha	Factor related to the slope of the water table	Grid
{domain}.beta	Factor related to the slope of the water table	Grid
{domain}.ct	Infiltration velocity at saturation	Grid
{domain}.fr	Soil fracturation	Grid
{domain}.cf	Field capacity	Grid
{domain}.cn	Curve Number	Grid
{domain}.ws	Water sources	Grid
{domain}.BareSoil	Bare soil mask	Grid
{domain}.Gd	Vegetation ET resistance factor	Grid
{domain}.Hveg	Average vegetation height	Grid
{domain}.RSmin	Minimum stomal resistance	Grid
{domain}.rfl	River depth (right)	Grid
{domain}.lfl	River depth (left)	Grid
{domain}.uc	Stream velocity in channel	Grid
{domain}.uh	Friction coefficient on hillslopes	Grid
{domain}.width	River width	Grid
{domain}.wt_max	Maximum capacity of the sub-surface reservoir	Grid
{domain}.info_dam	Main characteristics of the dams	Point
{domain}.info_lake	Main characteristics of the lakes	Point

Figure 1.

Figure S4: Examples of model static data for domain AFNW. From top left, clockwise, drainage direction, curve number, river width in meters and field capacity.

Discharge Quantiles

sample QQ-plots of discharge quantiles in some domains in East Africa. Each graph refers to a specific hydrological domain: on the x-axis the empirical sample quantiles, while on the y-axis the quantiles obtained from the selected fitted distributions.
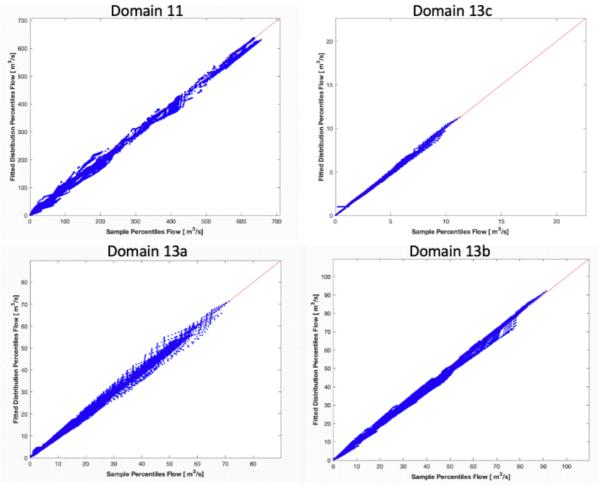

Figure S5: Comparison between empirical and fitted quantiles for different domains in East Africa.

This procedure was performed for the whole river network for the historical and future periods, leading to large set of fitted distribution of different families. Using the fitted distributions, the quantile values required for the Hydraulic simulation were computed.

Depending on the area considered, the analysis highlighted a severe increase in the extreme floods between historical and future periods (see for example Figure S6 where some results for the Kerala region in India are shown in particular for the 80th percentile future conditions SSP5 – RCP8.5).
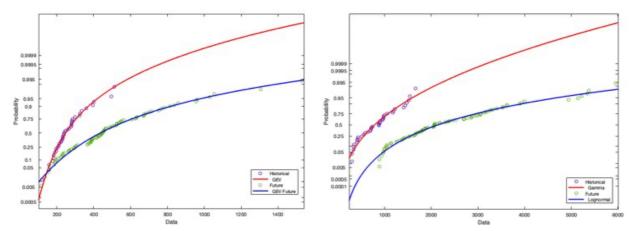

Figure S6: examples of comparison between the fitted probability distributions for historical discharge annual maxima (red) and future discharge annual maxima (blue): it is evident the strong increase in values. Kerala region, India.

Figure S7: Overall simulation workflow used to derive the inundation maps.

References

Andreadis, K. M., Schumann, G. J.-P., and Pavelsky, T.: A simple global river bankfull width and depth database, Water Resources Research, 49, 7164–7168, https://doi.org/10.1002/wrcr.20440, 2013.

ESA: Land Cover CCI Product User Guide Version 2. Tech. Rep., 2017.

Hengl, T., Jesus, J. M. de, Heuvelink, G. B. M., Gonzalez, M. R., Kilibarda, M., Blagotić, A., Shangguan, W., Wright, M. N., Geng, X., Bauer-Marschallinger, B., Guevara, M. A., Vargas, R., MacMillan, R. A., Batjes, N. H., Leenaars, J. G. B., Ribeiro, E., Wheeler, I., Mantel, S., and Kempen, B.: SoilGrids250m: Global gridded soil information based on machine learning, PLOS ONE, 12, e0169748, https://doi.org/10.1371/journal.pone.0169748, 2017.

Lehner, B., Liermann, C. R., Revenga, C., Vörösmarty, C., Fekete, B., Crouzet, P., Döll, P., Endejan, M., Frenken, K., Magome, J., Nilsson, C., Robertson, J. C., Rödel, R., Sindorf, N., and Wisser, D.: High-resolution mapping of the world's reservoirs and dams for sustainable river-flow management, Frontiers in Ecology and the Environment, 9, 494–502, https://doi.org/10.1890/100125, 2011.

Messager, M. L., Lehner, B., Grill, G., Nedeva, I., and Schmitt, O.: Estimating the volume and age of water stored in global lakes using a geo-statistical approach, Nat Commun, 7, 13603, https://doi.org/10.1038/ncomms13603, 2016.

Yamazaki, D., Ikeshima, D., Sosa, J., Bates, P. D., Allen, G. H., and Pavelsky, T. M.: MERIT Hydro: A High-Resolution Global Hydrography Map Based on Latest Topography Dataset, Water Resources Research, 55, 5053–5073, https://doi.org/10.1029/2019WR024873, 2019.